

Geophysical Research Letters

RESEARCH LETTER

10.1029/2020GL087163

Key Points:

- Multiphase flow leads to homogenization of rock dissolution and enhancement of mineral precipitation
- The identified pore-scale mechanisms have fundamental implications for soil weathering and subsurface applications
- The results provide a foundation for engineering design and predictive tools

Supporting Information:

- Supporting Information S1

Correspondence to:

J. Jiménez-Martínez,
jjimenez@ethz.ch;
joaquin.jimenez@eawag.ch

Citation:







Jimenez-Martinez, J., Hyman, J. D., Chen, Y., Carey, J. W., Porter, M. L., Kang, Q., et al. (2020). Homogenization of dissolution and enhanced precipitation induced by bubbles in multiphase flow systems. *Geophysical Research Letters*, 47, e2020GL087163. <https://doi.org/10.1029/2020GL087163>

Received 23 JAN 2020

Accepted 22 MAR 2020

Accepted article online 28 MAR 2020

Homogenization of Dissolution and Enhanced Precipitation Induced by Bubbles in Multiphase Flow Systems

Joaquín Jiménez-Martínez^{1,2} , Jeffrey D. Hyman³ , Yu Chen³ , J. William Carey³ , Mark L. Porter³, Qinqun Kang³ , George Guthrie Jr.³, and Hari S. Viswanathan³ 

¹Department of Water Resources and Drinking Water, Eawag, Dübendorf, Switzerland, ²Department of Civil, Environmental and Geomatic Engineering, ETH Zürich, Zürich, Switzerland, ³Earth & Environmental Sciences, Los Alamos National Laboratory, Los Alamos, NM, USA

Abstract Multiphase flow is ubiquitous in subsurface energy applications and natural processes, such as oil recovery, CO₂ sequestration, and water flow in soils. Despite its importance, we still lack a thorough understanding of the coupling of multiphase flow and reaction of transported fluids with the confining media, including rock dissolution and mineral precipitation. Through the use of geomaterial microfluidic flow experiments and high-performance computer simulations, we identify key pore-scale mechanisms that control this coupling. We compare the reactivity of fractured limestone with CO₂-saturated brine (single phase) and a mixture of supercritical (sc) CO₂ and CO₂-saturated brine (multiphase). We find that the presence of scCO₂ bubbles significantly changes both the flow dynamics and the resulting reaction patterns from a single-phase system, spatially homogenizing the rock dissolution. In addition, bubbles redirect oversaturated fluid into low-velocity regions, thereby enhancing carbonate precipitation occurs.

Plain Language Summary The impact of pore-scale multiphase flow on fluid-solid reactions is poorly understood because direct observations of reactive multiphase fluids in real rock materials are not widely available and the necessary computing is intractable. Using high-pressure/temperature geomaterial microfluidic experiments complemented by high-performance computer direct numerical simulation of multiphase flow in those geometries, we elucidate the pore-scale mechanisms that lead to homogenization of rock dissolution and enhancement of mineral precipitation. This study contributes to our ability to predict soil weathering and to optimize CO₂ sequestration and hydrocarbon extraction.

1. Introduction

Much has been conjectured about the pore-scale processes that govern multiphase flow and reaction in geologic systems, including rock dissolution and mineral precipitation. Direct observations of these processes under geological conditions are few, and the resulting uncertainty surrounding predictive calculations in subsurface systems limits our capacity to effectively produce hydrocarbon from conventional and unconventional resources (Hyman et al., 2016; Middleton et al., 2015), sequester CO₂ to limit greenhouse gas emissions (Lackner, 2003), determine weathering and nutrient availability in soils (Ciceri & Allanore, 2015; Maher & Chamberlain, 2014), among many important applications. Recent advances in experimental observations have begun to lift the veil shrouding our understanding of pore-scale phenomena, providing basic quantitative information needed to lay the foundations of a multiscale representation of flow and transport.

We now have temporally and 3-D spatially resolved observations of mineral dissolution patterns in porous materials that have revealed the evolution of capillary pressure properties (Krevor et al., 2011; Voltolini & Ajo-Franklin, 2019) and reaction rates (Menke et al., 2015), and in fractured materials, there are real-time observations of dissolution leading to channelization (Deng et al., 2015), heterogeneous reaction (Noiriel et al., 2013), and the interplay between shear fracture, aperture, shear displacement, and permeability (Frash et al., 2016, 2017). Microfluidics, a widely used technique, only recently has been applied at geological conditions through the development of high-pressure/temperature capable systems (Campbell & Orr, 1985; Jiménez-Martínez et al., 2016) and through the use of actual geologic materials as micromodels, which has allowed the investigation of wettability, matrix porosity, and mineral heterogeneity and thus greater fidelity

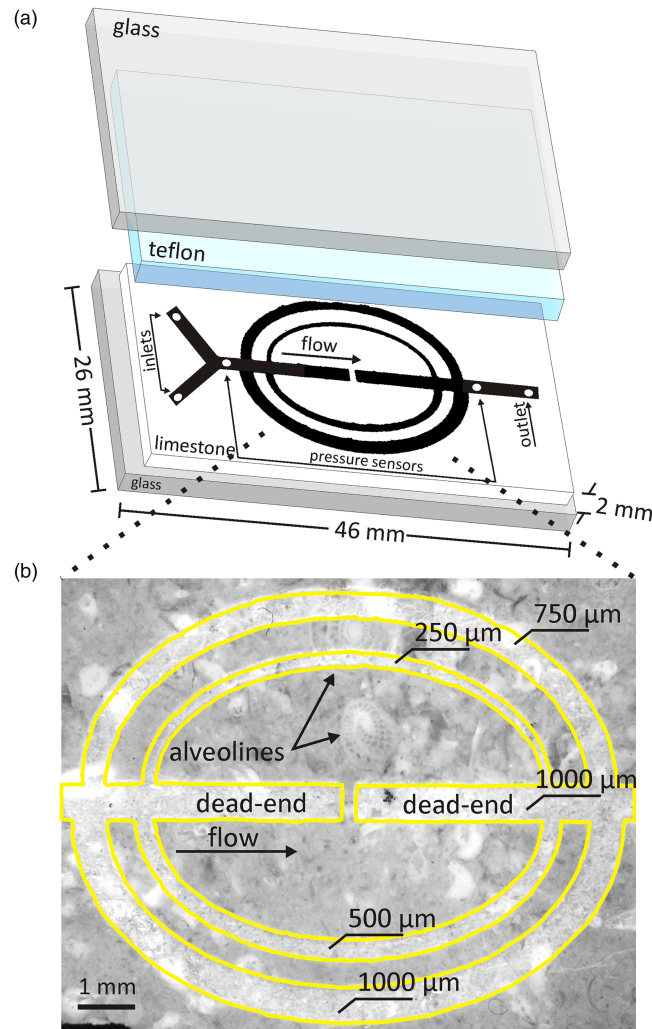


Figure 1. The geomaterial microfluidic device. (a) The chip is a sandwich of four layers: a glass plate, a thin layer of laser-etched limestone from the SACROC Unit (Texas, USA), Teflon™ for sealing, and an upper glass plate. The limestone layer contains the laser-etched microfluidic channels, the inlet and outlet ports, and the ports for pressure measurements. (b) Detail of the SACROC limestone layer indicating the widths of the etched channels, the main flow direction, and the fossil content, for example, foraminifera-alveolines. CO₂-saturated brine is injected at constant flow rate into the micromodel for the single-phase flow experiment. For the multiphase flow experiment, CO₂-saturated brine and scCO₂ are simultaneously pumped at equal constant flow rates into the micromodel.

of observations into subsurface processes (Ciceri & Allanore, 2015; Porter et al., 2015; Singh et al., 2017; Song et al., 2014). Simultaneously, there have been notable advances in high-performance computer (HPC) simulations of multiphase flow at unprecedented scales (Liu et al., 2016; Zhao et al., 2019). Supported by novel numerical discretization techniques, this fresh wave of simulations is allowing us to probe the fundamentals of these complicated phenomena in detail within complex geometries rather than idealized synthetic structures. Specifically, we can now use profilometry from microfluidic models and reproduce the experiments computationally in a unification that was not previously possible.

In this study, we integrate these recent developments in microfluidics and HPC multiphase simulations to characterize in a unique way spatially resolved differences in flow and reaction occurring in single-phase versus multiphase systems. Using limestone specimens with a system of channels mimicking variable fracture apertures, we quantify dissolution and precipitation during injection of single-phase brine and dissolved CO₂ and contrast that occurring with multiphase brine and supercritical (sc) CO₂ all at reservoir conditions. Reaction rates are deduced from changes in fracture morphology characterized by profilometry. We combine the experimental observations with HPC simulations of single-phase and multiphase flow conducted

in the profilometry-derived fracture geometry to quantify flow dynamics and reveal how the spatial distribution of discrete scCO₂ bubbles impacts relative rates of flow and reaction and how bubbles generate a pore-scale distribution of Damköhler number. Our results reveal the complex nature of multiphase flow and its pore-scale influence on fluid-solid reactions: homogenizes in space the solid dissolution and enhances local mineral precipitation. We discuss the pore-scale mechanisms that control them and the fundamental implications.

2. Materials and Methods

2.1. Experiments in Geomaterial Microfluidics

The purpose of these experiments is to characterize how the presence of discrete bubbles influences the organization of the flow field and in turn the spatial distribution of reactions. Our microfluidic device allows dissolution-precipitation reactions to be studied in a geomaterial micromodel fracture network containing fractures of different aperture. The microfluidic cell was fabricated from limestone core obtained from a well at the Scurry Area Canyon Reef Operators Committee Unit (SACROC Unit) (Texas, USA), a Pennsylvanian-age limestone reef (Carey et al., 2007; Raines & Helms, 2006). A fracture pattern was laser etched into the limestone micromodel, consisting of four curved channels and two dead-ends connected to a common inlet and outlet, with channel widths ranging from 250 to 1,000 μm and an average depth $\bar{d} \sim -150 \mu\text{m}$ (Figure 1). To quantify dissolution and precipitation rates, the micromodel was scanned before and after experiments by contactless high-resolution profilometry with a spatial (xy) resolution of 5.9 μm and vertical (z) resolution of 0.1 μm , and permeability was obtained experimentally (supporting information).

The microfluidic setup is sufficiently robust to allow experiments to be conducted under reservoir conditions; here, we use a temperature of 45 °C and pressure of 8.4 MPa. Two different protocols of fluid injection were followed: (i) single-phase experiments: A solution of brine saturated with CO₂ was pumped at constant flow rate into the micromodel for 87 hr, and (ii) multiphase experiments: Solutions consisting of the CO₂-saturated brine and scCO₂ (a very low miscible phase, i.e., behaving like an immiscible phase: 5-kg scCO₂/100-kg solvent; Dodds et al., 1956; Duan & Sun, 2003; Liu et al., 2012) were simultaneously pumped at equal constant flow rates into the micromodel for 90 hr. Total flow rates for the two protocols were the same (supporting information). In the multiphase experiments, the relative importance of capillary versus viscous forces can be quantified by the capillary number $Ca = \mu_{\text{brine}} u / (\sigma)$, where μ_{brine} is the viscosity of CO₂-saturated brine, σ is the surface tension at the interface between the two fluid phases (scCO₂ and CO₂-saturated brine) (Chiquet et al., 2007; Kvamme et al., 2007; Nielsen et al., 2012), and u the mean fluid flow velocity defined at the inlet channel. Ca is on the order of $\sim 10^{-5}$, with viscosity ratio $M = \mu_{\text{CO}_2} / \mu_{\text{brine}} \approx 5 \cdot 10^{-2}$, where μ_{CO_2} is the viscosity of scCO₂ (Lemmon et al., 2007; Nordbotten et al., 2005). Fluid properties at experimental conditions are summarized in Table S1. The pH of the CO₂-saturated brine solution was ~ 3 (Parkhurst & Appelo, 1999). Flow and transport were visualized by optical microscopy, and the pressure gradient was continuously monitored using a differential pressure transducer (Figure S1).

The chemical system of interest is the calcium carbonate-carbonic acid system (Plummer et al., 1978; Steefel et al., 2013). Calcite dissolves at relatively low pH in flowing regions, generating a relatively high concentration of the calcium ion. In turn, this diffuses into the relatively high pH of stagnant zones creating supersaturated conditions for calcite precipitation (supporting information). Therefore, the reactions taking place during the experiments are spatially heterogeneous due to varying flow rates and diffusion within the channels and the dead-end regions. The spatially distributed precipitation-dissolution rate can be quantified from profilometry data using a combined expression for precipitation (positive) and dissolution (negative):

$$r'(\mathbf{x}) = \frac{1}{v} \frac{\Delta H(\mathbf{x})}{\Delta t}, \quad (1)$$

with v (m^3/mol) the molar volume of calcite ($3.693 \times 10^{-5} \text{ m}^3/\text{mol}$), $\Delta H(\mathbf{x})$ (m) the height difference before and after the experiment (obtained by contactless high-resolution profilometry) at the location \mathbf{x} along the walls of the micromodel, and Δt (s) the duration of the experiment (Al-Khulaifi et al., 2017; Noiriel et al., 2016).

2.2. High-Performance Computing

The key focus of our experiments is to understand how multiphase flow leads to differences in reaction rates. While we could not observe the fluid velocity field in situ, we simulate the full-flow velocity field in the scanned geometries for both the single-phase and multiphase flow experiments using a highly optimized

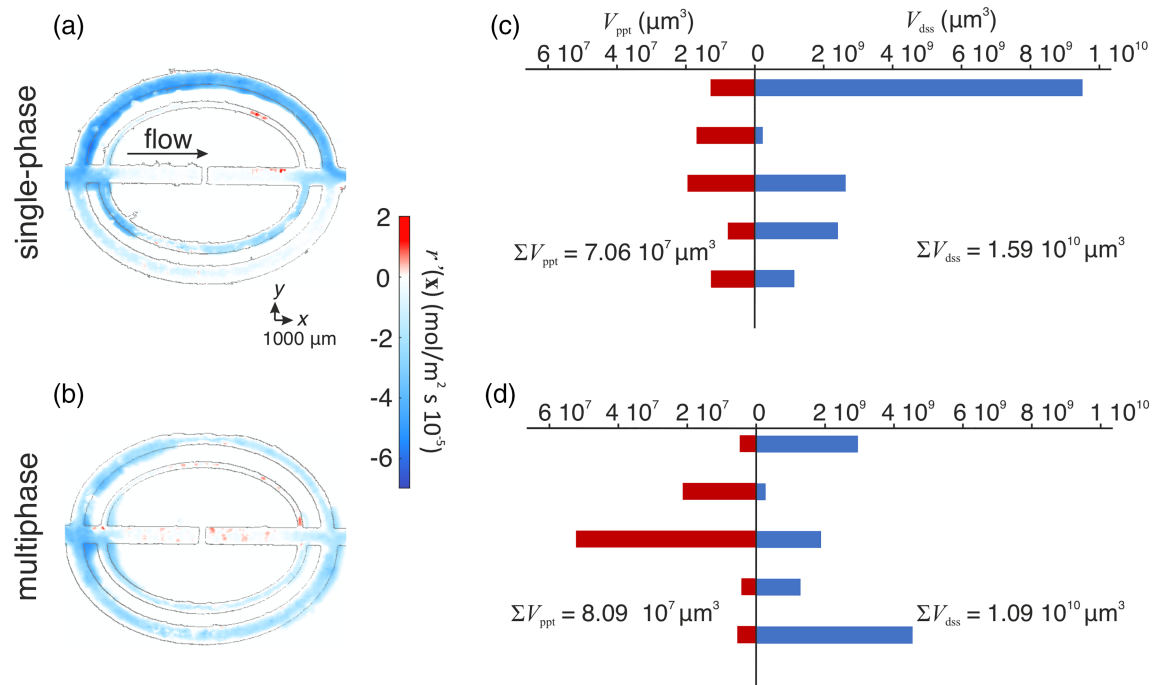


Figure 2. Rock dissolution and mineral precipitation in single-phase and multiphase flow conditions. (a, b) Combined reaction rate $r'(\mathbf{x})$ (equation (1)) (dissolution rate: negative values; precipitation rate: positive values) for both single-phase (a) and multiphase (b) flow experiments. Main flow direction is indicated. (c, d) Dissolved (V_{dss}) and precipitated (V_{ppt}) volumes in each of the channels including dead-ends in the single-phase (c) and multiphase (d) experiments. The vertical order of the bars in panels (c) and (d) corresponds to the vertical order channels (top to bottom) in panels (a) and (b). The total dissolved rock (ΣV_{dss}) and precipitated mineral volume (ΣV_{ppt}) for each experiment are also provided. Generally, multiphase flow homogenizes rock dissolution across channels and enhances mineral precipitation.

lattice Boltzmann (LB) method (Chen et al., 2018, 2019) run on HPC (Towns et al., 2014). The simulations were performed in the measured channel geometries at the beginning (t_0) and end (t_f) of the experiments, using the experimental measurement resolution and flow conditions. We used the velocity fields from the model to estimate the reaction potential throughout the micromodel and thus predict the rates of dissolution and distribution of precipitates.

The adopted LB methodology incorporates the continuum surface force (Brackbill et al., 1992) as a forcing term in the LB color-gradient multiphase model (Gunstensen et al., 1991) in a multiple-relaxation-rate framework (Lallemand & Luo, 2000) to reduce spurious currents, and an advanced wetting model allows us to accurately model wettability in the system (Leclaire et al., 2017). Each multiphase simulation contained $\mathcal{O}(10^{10})$ degrees of freedom and was run on $\mathcal{O}(10^3)$ cores requiring ≈ 40 hr of wall clock time.

3. Results

3.1. Dissolution and Precipitation Rates

$r'(\mathbf{x})$ (equation (1)) was calculated for both single-phase (Figure 2a) and multiphase (Figure 2b) flow experiments. Effective reaction rates for both precipitation $r_{\text{ppt}}|\{r' > 0\}$ and dissolution $r_{\text{dss}}|\{r' < 0\}$ were also computed. The effective dissolution rate was slightly lower in the multiphase than in the single-phase system, while the effective precipitation rate was higher (Table S2). In the single-phase experiment, the dissolution took place mainly in the channel of 750- μm width (Figure 2c). However, in the multiphase experiment, dissolution was more homogeneous in space, taking place more evenly across the three wider channels and in the central, close to the dead-end openings (Figure 2d). While precipitation was similar in all channels for the single-phase flow experiment, in the multiphase experiment, the opposite was true, with precipitation occurring principally in the dead-ends (Figures 2c and 2d). The total dissolved volume of limestone was higher in the single-phase experiment than in the multiphase experiment, while for precipitation was on the contrary (Figures 2c and 2d and Table S2).

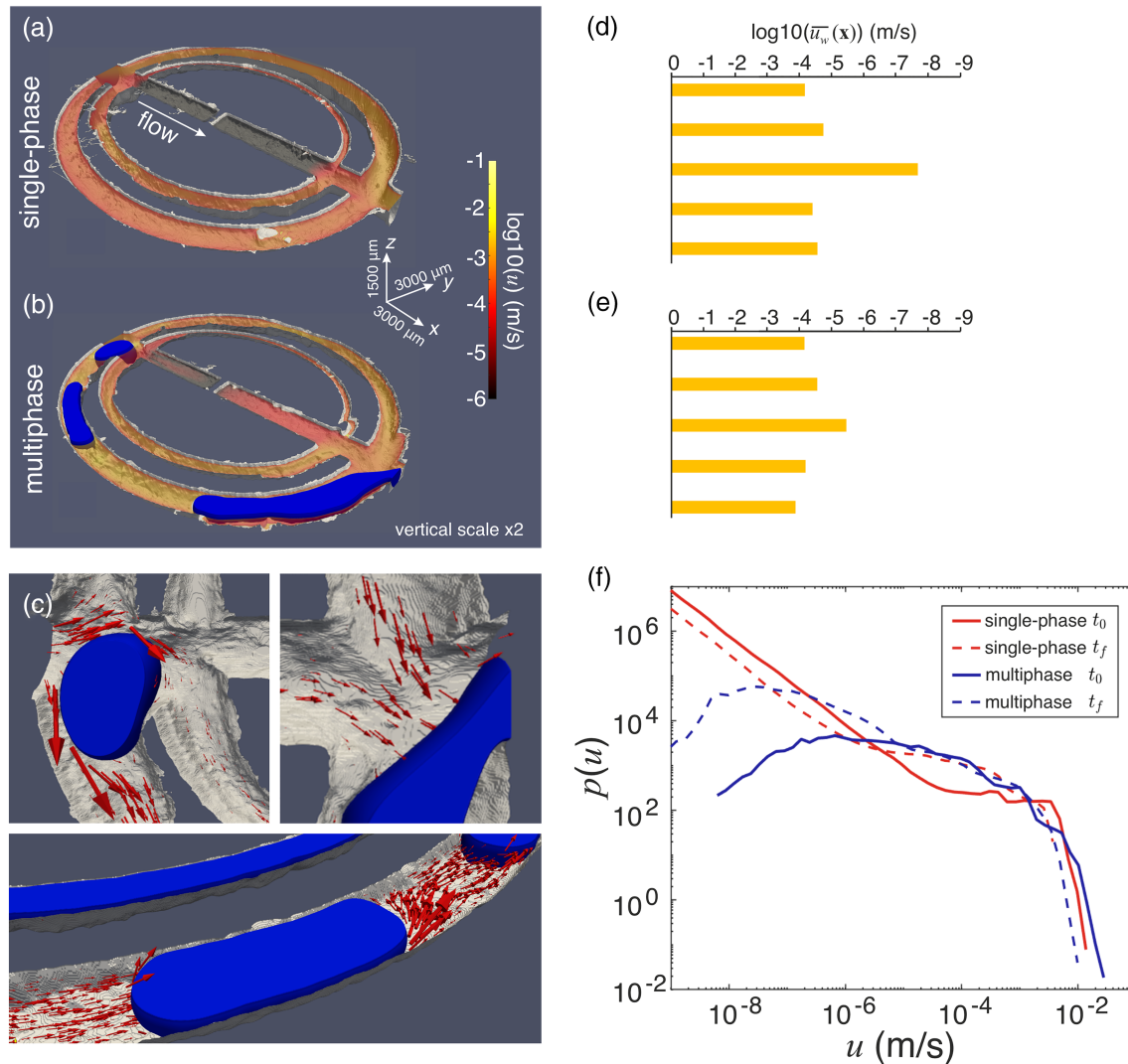


Figure 3. Fluid flow velocities in single-phase and multiphase flow conditions. (a, b) 3-D geomaterial micromodel geometries for single-phase and multiphase injections at t_f . The geometries were used in the single-phase and multiphase flow numerical simulations: Blue bubbles represent the scCO_2 , which are surrounded by the CO_2 -saturated brine (not shown). Vertical scale is exaggerated $\times 2$. The velocity field of the CO_2 -saturated brine at the midplane ($-75 \mu\text{m}$) is superimposed as color shading on the geometry. Main flow direction is indicated. (c) Velocity vectors showing the fluid being redirected due to a bubble (snapshots at the top correspond to the bubbles at the inlet and outlet in panel b; snapshots at the bottom correspond to the bubbles for the geometry at t_0). (d, e) Mean velocity of CO_2 -saturated brine at $8.5 \mu\text{m}$ from the limestone wall ($\overline{u_w}(\mathbf{x})$) in each channel, including the dead-ends. The vertical order of the bars in panels (d) and (e) corresponds to the vertical order channels (top to bottom) in panels (a) and (b). (f) Probability density functions of velocity ($p(u)$) in the CO_2 -saturated brine from the 3-D velocity data for both single-phase and multiphase injections at t_0 and t_f .

3.2. Structural and Phase Control on Flow Dynamics

The simulation results of multiphase flow and images of the experiments are in good agreement (Figure S2). The velocity field for brine at the midplane ($-75 \mu\text{m}$ from the surface) and t_f is shown in Figures 3a and 3b along with the 3-D resolved geometry. For the multiphase system, the distribution of CO_2 bubbles is shown in blue in Figure 3b. Rather than the bubbles flowing in a single (presumably largest) channel, we observed bubble movement among channels in both the experiments and the simulations (Movie S1). These dynamic changes in the flow field in the multiphase case, which are reflected in the time-dependent spatial distribution of scCO_2 bubbles, are driven by a competition between viscous and capillary forces. As bubbles reach the outlet, fluid flow is redirected into the dead-end channel (Figures 3b and 3c). We computed the mean velocity of brine at $8.5 \mu\text{m}$ from the limestone wall (the spatial resolution of the grid) within each channel (Figures 3d and 3e) which shows that for most of the channels, the flow velocity was the same in the two experiments, except in the dead-ends, where the velocity in the multiphase system is two orders of

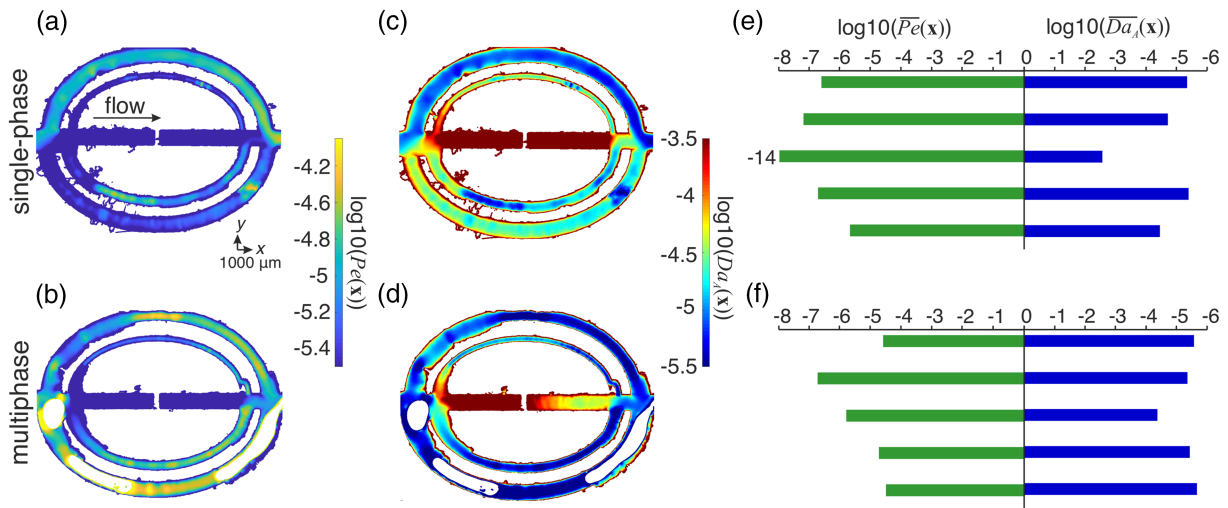


Figure 4. Transport versus reaction. Péclet number ($Pe(x) = Da_D/Da_A(x)$) field (a, b) and advective Damköhler number ($Da_A(x)$) field (c, d) at $8.5 \mu\text{m}$ from the limestone surface for single-phase and multiphase injections at t_f . (e, f) Mean $Pe(x)$ and $Da_A(x)$ at $8.5 \mu\text{m}$ from the limestone surface in each channel and in the central one, which includes both dead-ends, at t_f . The vertical order of the bars in panels (e) and (f) corresponds to the vertical order channels (top to bottom) in panels (a) and (c) and panels (b) and (d).

magnitude larger. This is reflected in the greater precipitation that occurs in these dead-end channels in the multiphase flow experiment than in the single-phase system (Figures 2d and 2e).

Simulations of single-phase flow in the prereaction geometries (i.e., t_0) of both the single-phase and multiphase experiments, showed very similar distributions of flow velocities, $p(u)$ (Figure S3). Therefore, the disparity in flow and reactions between the two experiments was due mainly to multiphase effects. We compare the $p(u)$ for the single-phase and multiphase systems at t_0 and t_f (Figure 3f). The presence of scCO_2 bubbles in the pore space clearly influences the velocity field of the CO_2 -saturated brine, broadening the $p(u)$ with higher velocities than in the single-phase case. Lower velocities are also expected in the multiphase case than in the single counterpart, because of the blocking of fluid flow in some regions (e.g., dead-ends) by scCO_2 bubbles (Jiménez-Martínez et al., 2017). However, the rearrangement of scCO_2 bubbles temporarily induces higher velocities in the dead-ends (Figure 3c). Both low and high velocities can be found in the CO_2 -saturated brine between the walls and scCO_2 bubbles, through film and corner flow (Figure 3c). Both single-phase and multiphase systems evolve to an overall lower flow velocity of CO_2 -saturated brine because of the limestone dissolution (Figure 3f).

3.3. The Balance of Transport and Reaction

The interplay between reaction kinetics and mass transport determines the dissolution and precipitation in the micromodels, governed by three main processes: (i) diffusion, (ii) advection, and (iii) reaction. The spatial variability of these processes is determined by the channel geometry, velocity of the fluid, concentration, and species' diffusion coefficients. Using the size of a calcite molecule as the characteristic length scale ($l = 4 \times 10^{-4} \mu\text{m}$), we can define a set of timescales associated with each of the three processes at the solid-fluid interface. The diffusion timescale, $\tau_D = l^2/(2D)$, is uniform throughout the domain, depending only on l and D , the molecular diffusion of CO_3^{2-} in CO_2 -saturated brine ($1.25 \times 10^{-9} \text{ m}^2/\text{s}$ at 45°C , $\sim \text{HCO}_3^-$) (Zeebe, 2011). Likewise, the reactive timescale, $\tau_R = l/(v_{\text{r}_{\text{dss}}})$, is also uniform throughout the domain. The advective timescale, $\tau_A(x) = l/u_w(x)$, however, depends on the spatially variable fluid velocity $u_w(x)$ close to the micromodel walls. We can obtain them from the simulations (Neuville et al., 2017). The relative balance of these forces can be quantified using the Damköhler number (Da), representing the ratio of transport to reaction timescales (Fredd & Fogler, 1998), and the Péclet number (Pe), which expresses the relative importance of advection versus diffusion. We define two Damköhler numbers, one diffusive $Da_D = \tau_D/\tau_R$ —also called the kinetic number (Golfier et al., 2002), the inverse of the Thiele modulus, a metric to quantify the potential diffusion limitation in reactions on surfaces (Thiele, 1939)—and one advective $Da_A(x) = \tau_A(x)/\tau_R$. According to the above definitions, Da_D has an isotropic character, since molecular diffusion and reaction are isotropic. In contrast, $Da_A(x)$ has an anisotropic character, since advection is directional. The Péclet number ($Pe(x) = \tau_D/\tau_A(x)$) can be expressed in terms of a ratio of Damköhler numbers ($Da_D/Da_A(x)$).

Plots of $Pe(\mathbf{x})$ and $Da_A(\mathbf{x})$ at 8.5 μm from the limestone surface highlight the spatial variability of these fields (Figures 4a and 4b and Figures 4c and 4d). In general, diffusion dominates over advection close to the channel edges (vertical walls), while the converse is true at the center of the channel. A comparison of the single-phase and multiphase experiments shows that $Pe(\mathbf{x})$ is more uniform (and higher) in the multiphase system, a consequence of more uniform and higher velocities. The spatial distribution of $Da_A(\mathbf{x})$ indicates diffusion-limited conditions in the dead-ends for the single-phase system. However, in the multiphase system, the dead-end adjacent to the outlet shows an advective contribution that, as previously discussed, results from redirection of brine flow due to the presence of scCO_2 bubbles. In general, the multiphase system is more transport limited than the single-phase system, due in part to the fact that the volumetric brine flow is one half that in the single-phase system. The average values of $Pe(\mathbf{x})$ and $Da_A(\mathbf{x})$ per channel demonstrate a homogenization of the velocity field resulting from the constant rearrangement of scCO_2 bubbles and the effect on the local $Pe(\mathbf{x})$ and $Da_A(\mathbf{x})$ values (Figures 4e and 4f).

4. Discussion

While at Darcy scale, uniform dissolution would be expected in both systems (Golfier et al., 2002), these experimental and computational observations demonstrate how local fluid-solid reactions are impacted by flow dynamics. In the single-phase experiment, dissolution took place mainly in the 750- μm width channel, indicating that therein the interplay between transport processes and the reactive phenomena, that is, $Da_A(\mathbf{x})$, was the favored for rock dissolution (Fredd et al., 1997). Although dissolution also took place, albeit to a lesser extent, in the rest of the micromodel, the highest velocities always occurred in the 750- μm width channel and resulted in enhanced dissolution and a trend toward wormhole formation. In the multiphase system, one would expect that the preferential flow of scCO_2 bubbles into larger channels due to capillary pressure would lead to less dissolution in the largest channels and greater dissolution (wormholing) in the smaller channels. However, this intuition proved incorrect. The dissolution rate was instead more homogeneous in the multiphase system, and there was no evidence of wormhole formation observed (Ott & Oedai, 2015; Soullaine et al., 2018). Instead, the bubbles of scCO_2 oscillated between the channels, continuously rearranging the flow field, so no runaway dissolution could occur and thereby making $Da_A(\mathbf{x})$ homogeneous across the channels. At the scale of these channels, capillary pressure was not a dominant force, allowing bubbles to move among the channels in response to more subtle dynamics imposed by temporal variations in fluid velocity and feedback with dissolution (Movies S1 and S2). The dynamic movement of scCO_2 bubbles was accompanied by dramatic changes of velocity in the CO_2 -saturated brine, in both magnitude and direction. The flow of CO_2 -saturated brine was mainly perturbed in the vicinity of scCO_2 bubbles before and after their actual displacement (Blois et al., 2015). When the bubbles were displaced because of local pressure variations, a relaxation in the pressure took place, aided by the compressibility of the bubbles, resulting in a backward movement of the bubbles. These back-and-forth movements induced recirculation in the CO_2 -saturated brine (Roman et al., 2016). This recirculating phenomena enhanced fluid-fluid mixing—destroying the concentration gradients observed in single-phase flow close to the walls (Deng et al., 2018). Mass transfer across the bubble-brine interface would refresh the CO_2 content of the brine. In this case, bubbles acted as conveyor of one of the reactants (Liu & Mostaghimi, 2018). These two bubble-related processes contribute to the homogenization of dissolution. An analysis of similarity between t_0 and t_f , using the Earth Mover's Distance method (Rubner et al., 2000) for the velocity of brine at 8.5 μm from the limestone wall, confirms the more spatially homogeneous dissolution in the multiphase system, not affecting the velocity distribution but only the magnitude (Table S3).

Just as the presence of scCO_2 bubbles limited flow in some areas, it redirected flow into others. Most notably, the bubbles redirected calcite-saturated brine into the dead-ends. In the single-phase experiment, the velocity in this region was so low that precipitation was diffusion limited. In contrast, these regions were the location of the highest precipitation in the multiphase experiment because the fluid was being constantly replenished by fluid with a higher calcite saturation (Zhou et al., 2019). We have no indication of the time required for nucleation in these regions, but the dependence of induction time on saturation index, which also depends on the precipitation mechanism (Prasianakis et al., 2017), suggests that it took on the order of day(s). Note that precipitation rate, that is, growth rate, is also expected to increase with saturation index and therefore with time (Berrezueta et al., 2017).

Under single-phase conditions, the measured effective dissolution rate for calcite (Table S2) is similar to the values in the literature for an acidic brine (pH ~ 3) (Al-Khulaifi et al., 2017; Neuville et al., 2017). The

observed effective dissolution rate is an order of magnitude lower than that measured on surfaces without transport limitations (Arvidson et al., 2003) and from batch experiments under similar experimental conditions (Peng et al., 2015), emphasizing how the flow field changes fluid-solid reactions. However, the reaction rate was likely not constant throughout the experiments. It was probably higher at early times due to a large surface roughness fracture (ratio between the total surface area and the nominal or geometric surface area) (Deng et al., 2018) and then stabilized at later times as this factor decreased due to dissolution (Al-Khulaifi et al., 2017).

In the multiphase experiment, brine forms a film between the scCO₂ bubbles and the limestone surface. As a result, despite the surface area between brine and rock not being significantly reduced compared with the single-phase system, the total volume of brine in the scCO₂-bearing channels is reduced, and thus, the total quantity of dissolved reactant, H₂CO₃, is reduced as well even though its consumption may be balanced by dissolution of CO₂ from the bubbles. Contrary to observations for fluid-fluid reactions, where the effective reaction rate increases with the presence of another immiscible phase in the porous space (Jiménez-Martínez et al., 2015, 2016), for fluid-solid reactions, the presence of a nonwetting immiscible or partially miscible phase may reduce the effective dissolution rate, even if the surface area in contact between the fluid and the solid is similar, because of the smaller volumetric flow.

As dissolution of the channel walls occurs, the porosity of the system increases, and in turn, the permeability also increases. The temporal dependence of permeability on porosity can be expressed as $\kappa_f = \kappa_0 (V_{pf}/V_{p0})^m$, where κ_i is the permeability, V_{pi} is the pore volume (subscripts f and 0 indicate final and initial time, respectively), and m is an empirical parameter. This dependence is strongly biased by sample anisotropy (Carroll et al., 2013; Civan, 2001). Using this power law, our experimental permeability results fit for $m \sim 1.5$, which is consistent with previous findings, indicating highly permeable limestone (Luquot & Gouze, 2009). However, for complex porous geometries, such relationships are nonunique: The evolution of the porous medium in time and in space dictates the relationship between porosity and permeability (Kang et al., 2014; Noguees et al., 2013). Our results indicate that in single-phase flow conditions, wormhole formation will be more pronounced and porosity/permeability increases will be fairly localized in high-velocity regions. In contrast, in a multiphase system, the dissolution will be disperse and the changes in porosity and permeability will be more uniformly distributed due to the constant rearrangement of the fluid velocity field by bubbles.

5. Conclusions

Through a combination of high-pressure/temperature microfluidic experiments and high-performance computer simulations, we have identified the key physical properties that control reactive flow in limestone for both single-phase CO₂-saturated brine flows and multiphase flow where bubbles of scCO₂ are present. In single-phase systems, fracture variability leads to preferential flow and enhanced dissolution, creating a runaway dissolution effect (wormholing). Contrary to expectations, the multiphase system was more homogeneous in both flow and dissolution, with an absence of wormhole behavior. This homogenization was driven by bubbles of scCO₂ alternating among the channels (rather than occupying the largest channel) and probably also because of reduced transport barriers facilitated by mass transfer between scCO₂ bubbles and the surrounding brine film. The scCO₂ bubbles also redirected flow so that saturated fluid entered dead-end channels, leading to calcite precipitation. The constantly changing velocity field enhanced mixing, renewing fresh solution in contact with the solid walls. By using a combination of microscopic observations of dissolution and precipitation with numerical simulation of multiphase flow, we obtained a detailed spatial map of the connection between pore-scale processes and macroscopic behavior. The results reveal counterintuitive reaction and flow mechanisms in multiphase systems that point the way toward physically based upscaling strategies of fluid-solid reactions in multiphase flow systems.

References

- Al-Khulaifi, Y., Lin, Q., Blunt, M. J., & Bijeljic, B. (2017). Reaction rates in chemically heterogeneous rock: Coupled impact of structure and flow properties studied by X-ray microtomography. *Environmental Science & Technology*, 51(7), 4108–4116.
- Arvidson, R. S., Ertan, I. E., Amonette, J. E., & Luttge, A. (2003). Variation in calcite dissolution rates: A fundamental problem? *Geochimica et Cosmochimica Acta*, 67(9), 1623–1634.
- Berrezueta, E., Kovacs, T., & Luquot, L. (2017). Qualitative and quantitative changes of carbonate rocks exposed to SC CO₂ (Basque-Cantabrian Basin, Northern Spain). *Applied Sciences*, 7(11), 1124.
- Blois, G., Barros, J. M., & Christensen, K. T. (2015). A microscopic particle image velocimetry method for studying the dynamics of immiscible liquid–liquid interactions in a porous micromodel. *Microfluidics and Nanofluidics*, 18(5-6), 1391–1406.

Acknowledgments

This project is supported by the Department of Energy (DOE) Basic Energy Sciences program (DE-AC52-06NA25396 and FWP# LANL20171450), Laboratory Directed Research and Development (20140002DR), and Institutional Computing Program. We used the Extreme Science and Engineering Discovery Environment (XSEDE), supported by the National Science Foundation Grant ACI-1548562, and the TACC Stampede2 system (allocation ID: EAR160028). J. J.-M. gratefully acknowledges financial support from the Swiss National Science Foundation (SNSF, Grant 200021_178986) and Eawag Discretionary Funding. We thank Lazaro Perez and one anonymous reviewer for their insightful and constructive comments. Data archiving is underway in the institutional open-access repository (<https://polybox.ethz.ch/index.php/s/x8jFWMNw7tLfuB8>).

- Brackbill, J. U., Kothe, D. B., & Zemach, C. (1992). A continuum method for modeling surface tension. *Journal of Computational Physics*, 100(2), 335–354.
- Campbell, B. T., & Orr, F. M. (1985). Flow visualization for CO₂/crude-oil displacements. *SPE Journal*, 25(05), 665–678.
- Carey, J. W., Wigand, M., Chipera, S. J., WoldeGabriel, G., Pawar, R., Lichtner, P. C., et al. (2007). Analysis and performance of oil well cement with 30 years of CO₂ exposure from the SACROC Unit, West Texas, USA. *International Journal of Greenhouse Gas Control*, 1(1), 75–85.
- Carroll, S., Hao, Y., Smith, M., & Sholokhova, Y. (2013). Development of scaling parameters to describe CO₂-rock interactions within Weyburn-Midale carbonate flow units. *International Journal of Greenhouse Gas Control*, 16, S185–S193.
- Chen, Y., Li, Y., Valocchi, A. J., & Christensen, K. T. (2018). Lattice Boltzmann simulations of liquid CO₂ displacing water in a 2D heterogeneous micromodel at reservoir pressure conditions. *Journal of Contaminant Hydrology*, 212, 14–27.
- Chen, Y., Valocchi, A. J., Kang, Q., & Viswanathan, H. S. (2019). Inertial effects during the process of supercritical CO₂ displacing brine in a sandstone: Lattice Boltzmann simulations based on the continuum-surface-force and geometrical wetting models. *Water Resources Research*, 55, 11,144–11,165. <https://doi.org/10.1029/2019WR025746>
- Chiquet, P., Darion, J. C., Broseta, D., & Thibeau, S. (2007). CO₂/water interfacial tensions under pressure and temperature conditions of CO₂ geological storage. *Energy Conversion and Management*, 48, 736–744. <https://doi.org/10.1016/j.enconman.2006.09.011>
- Ciceri, D., & Allanore, A. (2015). Microfluidic leaching of soil minerals: Release of K⁺ from K feldspar. *PLoS one*, 10(10), e0139979.
- Civan, F. (2001). Scale effect on porosity and permeability: Kinetics, model, and correlation. *AIChE Journal*, 47(2), 271–287.
- Deng, H., Fitts, J. P., Crandall, D., McIntyre, D., & Peters, C. A. (2015). Alterations of fractures in carbonate rocks by CO₂-acidified brines. *Environmental Science & Technology*, 49(16), 10,226–10,234.
- Deng, H., Molins, S., Trebotich, D., Steefel, C., & DePaolo, D. (2018). Pore-scale numerical investigation of the impacts of surface roughness: Upscaling of reaction rates in rough fractures. *Geochimica et Cosmochimica Acta*, 239, 374–389.
- Dodds, W. S., Stutzman, L. F., & Sollami, B. J. (1956). Carbon dioxide solubility in water. *Industrial & Engineering Chemistry*, 1, 92–95. <https://doi.org/10.1021/i460001a018>
- Duan, Z., & Sun, R. (2003). An improved model calculating CO₂ solubility in pure water and aqueous NaCl solutions from 273 to 533 K and from 0 to 2000 bar. *Chemical Geology*, 193, 257–271. [https://doi.org/10.1016/S0009-2541\(02\)00263-2](https://doi.org/10.1016/S0009-2541(02)00263-2)
- Frash, L. P., Carey, J. W., Ickes, T., & Viswanathan, H. S. (2017). Caprock integrity susceptibility to permeable fracture creation. *International Journal of Greenhouse Gas Control*, 64, 60–72.
- Frash, L. P., Carey, J. W., Lei, Z., Rougier, E., Ickes, T., & Viswanathan, H. S. (2016). High-stress triaxial direct-shear fracturing of utica shale and in situ X-ray microtomography with permeability measurement. *Journal of Geophysical Research: Solid Earth*, 121, 5493–5508. <https://doi.org/10.1002/2016JB012850>
- Fredd, C. N., & Fogler, H. S. (1998). Influence of transport and reaction on wormhole formation in porous media. *AIChE Journal*, 44(9), 1933–1949.
- Fredd, C. N., Tjia, R., & Fogler, H. S. (1997). The existence of an optimum Damkohler number for matrix stimulation of carbonate formations. In *Spe European Formation Damage Conference*. Society of Petroleum Engineers.
- Golfier, F., Zarcone, C., Bazin, B., Lenormand, R., Lasseux, D., & Quintard, M. (2002). On the ability of a Darcy-scale model to capture wormhole formation during the dissolution of a porous medium. *Journal of Fluid Mechanics*, 457, 213–254.
- Gunsten, A. K., Rothman, D. H., Zaleski, S., & Zanetti, G. (1991). Lattice Boltzmann model of immiscible fluids. *Physical Review A*, 43(8), 4320.
- Hyman, J. D., Jiménez-Martínez, J., Viswanathan, H. S., Carey, J. W., Porter, M. L., Rougier, E., et al. (2016). Understanding hydraulic fracturing: A multi-scale problem. *Philosophical Transactions of the Royal Society A*, 374(2078), 20150426.
- Jiménez-Martínez, J., de Anna, P., Tabuteau, H., Turuban, R., Le Borgne, T., & Méheust, Y. (2015). Pore-scale mechanisms for the enhancement of mixing in unsaturated porous media and implications for chemical reactions. *Geophysical Research Letters*, 42, 5316–5324. <https://doi.org/10.1002/2015GL064513>
- Jiménez-Martínez, J., Le Borgne, T., Tabuteau, H., & Méheust, Y. (2017). Impact of saturation on dispersion and mixing in porous media: Photobleaching pulse injection experiments and shear-enhanced mixing model. *Water Resources Research*, 53, 1457–1472. <https://doi.org/10.1002/2016WR019849>
- Jiménez-Martínez, J., Porter, M. L., Hyman, J. D., Carey, J. W., & Viswanathan, H. S. (2016). Mixing in a three-phase system: Enhanced production of oil-wet reservoirs by CO₂ injection. *Geophysical Research Letters*, 42, 196–205. <https://doi.org/10.1002/2015GL066787>
- Kang, Q., Chen, L., Valocchi, A. J., & Viswanathan, H. S. (2014). Pore-scale study of dissolution-induced changes in permeability and porosity of porous media. *Journal of Hydrology*, 517, 1049–1055.
- Krevor, S. C. M., Pini, R., Li, B., & Benson, S. M. (2011). Capillary heterogeneity trapping of CO₂ in a sandstone rock at reservoir conditions. *Geophysical Research Letters*, 38, L15401. <https://doi.org/10.1029/2011GL048239>
- Kvamme, B., Kuznetsova, T., Hebach, A., Oberhof, A., & Lunde, E. (2007). Measurements and modelling of interfacial tension for water plus carbon dioxide systems at elevated pressures. *Computational Materials Science*, 38, 506–513.
- Lackner, K. S. (2003). A guide to CO₂ sequestration. *Science*, 300(5626), 1677–1678.
- Lallemand, P., & Luo, L.-S. (2000). Theory of the lattice Boltzmann method: Dispersion, dissipation, isotropy, Galilean invariance, and stability. *Physical Review E*, 61(6), 6546.
- Leclaire, S., Parmigiani, A., Malaspinas, O., Chopard, B., & Latt, J. (2017). Generalized three-dimensional lattice Boltzmann color-gradient method for immiscible two-phase pore-scale imbibition and drainage in porous media. *Physical Review E*, 95(3), 033,306.
- Lemmon, E. W., McLinden, M. O., & Huber, M. L. (2007). REFPROP: Reference fluid thermodynamic and transport properties. NIST Standard Reference Database 23 (8.0).
- Liu, N., Aymonier, C., Lecoutre, C., Garrabos, Y., & Marre, S. (2012). Microfluidic approach for studying CO₂ solubility in water and brine using confocal Raman spectroscopy. *Chemical Physics Letters*, 551, 139–143. <https://doi.org/10.1016/j.cplett.2012.09.007>
- Liu, H., Kang, Q., Leonardi, C. R., Schmieschek, S., Narváez, A., Jones, B. D., et al. (2016). Multiphase lattice Boltzmann simulations for porous media applications. *Computational Geosciences*, 20(4), 777–805.
- Liu, M., & Mostaghimi, P. (2018). Numerical simulation of fluid-fluid-solid reactions in porous media. *International Journal of Heat and Mass Transfer*, 120, 194–201.
- Luquot, L., & Gouze, P. (2009). Experimental determination of porosity and permeability change induced by injection of CO₂ into carbonate rocks. *Chemical Geology*, 265(1), 148–159.
- Maher, K., & Chamberlain, C. P. (2014). Hydrologic regulation of chemical weathering and the geologic carbon cycle. *Science*, 343(6178), 1502–1504.
- Menke, H. P., Bijeljic, B., Andrew, M. G., & Blunt, M. J. (2015). Dynamic three-dimensional pore-scale imaging of reaction in a carbonate at reservoir conditions. *Environmental Science & Technology*, 49(7), 4407–4414.

- Middleton, R. S., Carey, J. W., Currier, R. P., Hyman, J. D., Kang, Q., Karra, S., et al. (2015). Shale gas and non-aqueous fracturing fluids: Opportunities and challenges for supercritical CO₂. *Applied Energy*, 147, 500–509.
- Neuville, A., Renaud, L., Luu, T. T., Minde, M. W., Jettstuen, E., Vinningland, J. L. G., et al. (2017). Xurography for microfluidics on a reactive solid. *Lab Chip*, 17(2), 293–303.
- Nielsen, L. C., Bourg, I. C., & Sposito, G. (2012). Predicting CO₂–water interfacial tension under pressure and temperature conditions of geologic CO₂ storage. *Geochimica et Cosmochimica Acta*, 81, 28–38. <https://doi.org/10.1016/j.gca.2011.12.018>
- Nogues, J. P., Fitts, J. P., Celia, M. A., & Peters, C. A. (2013). Permeability evolution due to dissolution and precipitation of carbonates using reactive transport modeling in pore networks. *Water Resources Research*, 49, 6006–6021. <https://doi.org/10.1002/wrcr.20486>
- Noiriel, C., Gouze, P., & Madé, B. (2013). 3D analysis of geometry and flow changes in a limestone fracture during dissolution. *Journal of Hydrology*, 486, 211–223.
- Noiriel, C., Steefel, C. I., Yang, L., & Bernard, D. (2016). Effects of pore-scale precipitation on permeability and flow. *Advances in Water Resources*, 95, 125–137.
- Nordbotten, J. M., Celia, M. A., & Bachu, S. (2005). Injection and storage of CO₂ in deep saline aquifers: Analytical solution for CO₂ plume evolution during injection. *Transport Porous Media*, 58(3), 339–360. <https://doi.org/10.1007/s11242-004-0670-9>
- Ott, H., & Oedai, S. (2015). Wormhole formation and compact dissolution in single- and two-phase CO₂-brine injections. *Geophysical Research Letters*, 42, 2270–2276. <https://doi.org/10.1002/2015GL063582>
- Parkhurst, D. L., & Appelo, C. A. J. (1999). *User's guide to PHREEQC (Version 2): A computer program for speciation, batch-reaction, one-dimensional transport, and inverse geochemical calculations*. Denver, CO: US Geological Survey.
- Peng, C., Crawshaw, J. P., Maitland, G. C., & Trusler, J. P. M. (2015). Kinetics of calcite dissolution in CO₂-saturated water at temperatures between (323 and 373) K and pressures up to 13.8 MPa. *Chemical Geology*, 403, 74–85.
- Plummer, L. N., Wigley, T. M. L., & Parkhurst, D. L. (1978). The kinetics of calcite dissolution in CO₂-water systems at 5° to 60° C and 0.0 to 1.0 atm CO₂. *American Journal of Science*, 278(2), 179–216.
- Porter, M. L., Jiménez-Martínez, J., Martínez, R., McCulloch, Q., Carey, J. W., & Viswanathan, H. S. (2015). Geo-material microfluidics at reservoir conditions for subsurface energy resource applications. *Lab Chip*, 15, 4044–4053.
- Prasianakis, N. I., Curti, E., Kosakowski, G., Poonosamy, J., & Churakov, S. V. (2017). Deciphering pore-level precipitation mechanisms. *Scientific Reports*, 7(1), 13,765.
- Raines, M., & Helms, W. (2006). Non-standard core analysis applied to geologic model generation for fluid flow simulation. *Publications-West Texas Geological Society*, 115, 123.
- Roman, S., Soullaine, C., AlSaud, M. A., Kovscek, A., & Tchepeli, H. (2016). Particle velocimetry analysis of immiscible two-phase flow in micromodels. *Advances in Water Resources*, 95, 199–211.
- Rubner, Y., Tomasi, C., & Guibas, L. J. (2000). The earth mover's distance as a metric for image retrieval. *International Journal of Computer Vision*, 40(2), 99–121.
- Singh, R., Sivaguru, M., Fried, G. A., Fouke, B. W., Sanford, R. A., Carrera, M., & Werth, C. J. (2017). Real rock-microfluidic flow cell: A test bed for real-time in situ analysis of flow, transport, and reaction in a subsurface reactive transport environment. *Journal of Contaminant Hydrology*, 204, 28–39.
- Song, W., de Haas, T. W., Fadaei, H., & Sinton, D. (2014). Chip-off-the-old-rock: The study of reservoir-relevant geological processes with real-rock micromodels. *Lab Chip*, 14(22), 4382–4390. <https://doi.org/10.1039/c4lc00608a>
- Soullaine, C., Roman, S., Kovscek, A., & Tchepeli, H. A. (2018). Pore-scale modelling of multiphase reactive flow: Application to mineral dissolution with production of CO₂. *Journal of Fluid Mechanics*, 855, 616–645.
- Steefel, C. I., Molins, S., & Trebotich, D. (2013). Pore scale processes associated with subsurface CO₂ injection and sequestration. *Reviews in Mineralogy and Geochemistry*, 77(1), 259–303.
- Thiele, E. W. (1939). Relation between catalytic activity and size of particle. *Industrial & Engineering Chemistry Research*, 31(7), 916–920.
- Towns, J., Cockerill, T., Dahan, M., Foster, I., Gaither, K., Grimshaw, A., et al. (2014). XSEDE: Accelerating scientific discovery. *Computing in Science & Engineering*, 16(5), 62–74.
- Voltolini, M., & Ajo-Franklin, J. (2019). The effect of CO₂-induced dissolution on flow properties in Indiana Limestone: An in situ synchrotron x-ray micro-tomography study. *International Journal of Greenhouse Gas Control*, 82, 38–47.
- Zeebe, R. E. (2011). On the molecular diffusion coefficients of dissolved CO₂, HCO₃[−], and CO₃^{2−} and their dependence on isotopic mass. *Geochimica et Cosmochimica Acta*, 75(9), 2483–2498.
- Zhao, B., MacMinn, C. W., Primkulov, B. K., Chen, Y., Valocchi, A. J., Zhao, J., et al. (2019). Comprehensive comparison of pore-scale models for multiphase flow in porous media. *Proceedings of the National Academy of Sciences*, 116(28), 13,799–13,806.
- Zhou, J. Q., Wang, L., Chen, Y. F., & Cardenas, M. B. (2019). Mass transfer between recirculation and main flow zones: Is physically-based parameterization possible? *Water Resources Research*, 55, 345–362. <https://doi.org/10.1029/2018WR023124>